The proposed protective biological function of PIF1 may have emerged early in angiosperm evolution to provide a selective advantage in certain environments where seed burial was critical to survival. The capacity to germinate and emerge from subterranean darkness may have been particularly important in the successful radiation of the seed producers into drier, more hostile environments. Seed burial can provide long-term survival through protection from predators and hostile surface conditions until environmental conditions are favorable for germination and can facilitate establishment of a robust underground root system before seedling emergence, thereby increasing survival potential.

phy signaling through a bHLH transcriptional network. The reverse-genetic strategy of targeting *Arabidopsis* bHLH-family members, which are phylogenetically related to PIF3, for potential involvement in phy-regulated development is providing emerging evidence of a small network of these factors differentially involved in regulating and integrating different facets of the seedling deetiolation process. PIF3 (*11*), PIF4 (*16*), HFR1 (*17*), PIL1 (*18*), and PIF1 are all involved in this process, but each appears to have a differential role. Moreover, together with the recent evidence of phy-induced PIF3 degradation (*14*), our data here for PIF1 suggest that modulation of constitutively active transcription factor activity might be one of the mechanisms by which the phy family of photoreceptors induces photomorphogenesis in response to light.

References and Notes

1. S. Reinbothe, C. Reinbothe, K. Apel, N. Lebedev, *Cell* **86**, 703 (1996).
2. R. G. L. op den Camp *et al.*, *Plant Cell* **15**, 2320 (2003).
3. P. H. Quail, *Nature Rev. Mol. Cell. Biol.* **3**, 85 (2002).
4. H. Wang, X.-W. Deng, *The Arabidopsis Book*, C. R. Somerville, E. M. Meyerowitz, Eds. (American Society of Plant Biologists, Rockville, MD, 2004), 10.1199/tab.0074.1, http://aspb.org/publications/arabidopsis.
5. M. M. Neff, C. Fankhauser, J. Chory, *Genes Dev.* **14**, 257 (2000).
6. P. H. Quail, *Sem. Cell Dev. Biol.* **11**, 457 (2000).
7. F. Nagy, E. Schaefer, *Annu. Rev. Plant Biol.* **53**, 329 (2002).
8. S. Kircher *et al.*, *Plant Cell* **14**, 1541 (2002).
9. J. Martinez-Garcia, E. Huq, P. H. Quail, *Science* **288**, 859 (2000).
10. M. Ni, J. M. Tepperman, P. H. Quail, *Nature* **400**, 781 (1999).
11. M. Ni, J. M. Tepperman, P. H. Quail, *Cell* **95**, 657 (1998).
12. K. J. Halliday, M. Hudson, M. Ni, M.-M. Qin, P. H. Quail, *Proc. Natl. Acad. Sci. U.S.A.* **96**, 5832 (1999).
13. J. Kim *et al.*, *Plant Cell* **15**, 2399 (2003).
14. D. Bauer *et al.*, *Plant Cell* **16**, 1433 (2004).
15. E. Monte, P. Quail, unpublished data.
16. E. Huq, P. H. Quail, *EMBO J.* **21**, 2441 (2002).
17. C. D. Fairchild, M. A. Schumaker, P. H. Quail, *Genes Dev.* **14**, 2377 (2000).
18. M. G. Salter, F. A. Keara, G. C. Whitelam, *Nature* **426**, 680 (2003).
19. R. Meskauskiene *et al.*, *Proc. Natl. Acad. Sci. U.S.A.* **98**, 12826 (2001).
20. E. Huq, P. H. Quail, data not shown.
21. Y. Zhu, J. M. Tepperman, C. D. Fairchild, P. H. Quail, *Proc. Natl. Acad. Sci. U.S.A.* **97**, 13419 (2000).
22. Materials and methods are available as supporting material on *Science* Online.
23. W. P. Inskeep, P. R. Bloom, *Plant Physiol.* **77**, 483 (1985).

24. We thank K. Chang and C. Lanzatella for technical assistance, J. Tepperman for help with nuclear localization assays, V. Symonds for help with photography, and the *Arabidopsis* Biological Resource Center, Ohio, for providing seed stocks. Supported by grants from NIH no. GM47475, the Torrey Mesa Research Institute, San Diego, U.S. Department of Energy Basic Energy Sciences no. DE-FG03-87ER13742 and U.S. Department of Agriculture Current Research Information Service no. 5335-21000-010-00D to P.H.Q. and a set-up fund from University of Texas at Austin to E. H. Molecular interaction data have been deposited in the Biomolecular Interaction Network Database with accession codes 151737, 151738, 151739, and 151740.

Supporting Online Material

www.sciencemag.org/cgi/content/full/305/5692/1937/DC1
Materials and Methods
Figs. S1 to S5
References

28 April 2004; accepted 4 August 2004

REPORTS

Observation of Superflow in Solid Helium

E. Kim and M. H. W. Chan*

We report on the observation of nonclassical rotational inertia in solid helium-4 confined to an annular channel in a sample cell under torsional motion, demonstrating superfluid behavior. The effect shows up as a drop in the resonant oscillation period as the sample cell is cooled below 230 millikelvin. Measurement of 17 solid samples allows us to map out the boundary of this superfluid-like solid or supersolid phase from the melting line up to 66 bars. This experiment indicates that superfluid behavior is found in all three phases of matter.

At temperatures below 2.176 K, liquid ^{4}He enters into a superfluid state and flows without any friction (*1*, *2*). The onset of superfluidity is associated with Bose-Einstein condensation (*3*, *4*), where the ^{4}He atoms, which are bosons, condense into a single momentum state and acquire quantum mechanical coherence over macroscopic length scales. Bose-Einstein condensation of alkali atoms in the vapor phase was achieved (*5*) in 1995, and there is strong evidence for superfluidity in these systems (*6*–*8*). Perhaps counter to intuition, superfluid-like behavior is thought possible even in solid helium (*9*–*14*). A recent torsional oscillator measurement found evidence of superfluid flow in solid helium confined in porous Vycor glass (*15*) with pore diameter of 7 nm. There is, however, concern that the observed effect may be due to a liquid-like layer of helium atoms adsorbed on the surface of the pores (*16*). Here we report observation of superflow in bulk solid helium. Our experiment shows that the superfluid-like behavior is a general and intrinsic property of solid helium and not the result of confinement in any particular medium.

The resonant period of the high mechanical quality factor torsional oscillator (*17*) (Fig. 1) is given by $2\pi[(I/G)^{1/2}]$, where I is the moment of inertia of the torsion cell, which contains ^{4}He, and G is the torsion spring constant of the Be-Cu torsion rod. The torsion cell has an annular channel in which ^{4}He can be introduced and pressurized to the solid phase. Ultrahigh-purity ^{4}He, with a stated ^{3}He impurity of 0.3 parts per million, is used in our experiment. When ^{4}He enters the superfluid or supersolid phase and acquires nonclassical rotational inertia (NCRI), a fraction of the helium decouples from the oscillation, thereby reducing the rotational inertia I and the resonant period. We have measured a total of 17 solid ^{4}He samples with pressure ranging from 26 bars, close to the melting boundary, to 66 bars; all showed supersolid decoupling below 230 mK.

The resonant period as a function of temperature is shown for a solid sample pressurized to 51 bars (Fig. 2A). Measurements

Department of Physics, Pennsylvania State University, University Park, PA 16802, USA.

*To whom correspondence should be addressed. E-mail: chan@phys.psu.edu

were made with different drive voltages, inducing different amplitudes and speeds of oscillation. We calculated and labeled the different runs by the maximum speed in a cycle of oscillation as computed at the mean radius of the annular channel, v_{max}. We display our data on a logarithmic rather than a linear scale to better highlight results in the low-temperature region. The resonant period showed a linear dependence on temperature from 0.3 K up to 1.5 K. A linear dependence on temperature extending down to 0.1 K, with a shallower slope, was also found for the empty cell. The empty-cell period is smaller than the filled-cell value by 3012 ns at 0.3 K. When the lock-in amplifier is adjusted for measurement with a different oscillation speed, the resonant period often shows a shift of a few ns. However, the period versus temperature curves for different speeds have identical slopes and can be made to collapse onto each other, as shown in the figure, by shifting the period values at any temperature between 0.3 and 1.5 K.

Below 250 mK, the period begins to drop below the linear background extrapolated from higher temperature. The negative period shift, or the difference between the measured period and the period given by linear background ($\tau - \tau^*$), increases smoothly but rapidly with decreasing temperature and saturates below 40 mK. The resonant period curves measured with v_{max} equal to 4 and 6 μm/s are identical and appear as a single curve down to the lowest temperature. At 14 μm/s and above, the period shift decreases with v_{max} and falls below the level of detection for the run with v_{max} equal to 420 μm/s.

Although a constant ac voltage was used to excite the oscillation for each run of a specific v_{max}, a broad minimum in the amplitude of the oscillation (and hence also v_{max}) is seen over the temperature range where $\tau - \tau^*$ is changing most rapidly. This minimum is seen for all solid samples studied, irrespective of the oscillating speed. For clarity we show in Fig. 2A the amplitude curves for only three runs, namely with v_{max} at 4, 33, and 117 μm/s. In some runs, the low-temperature amplitude recovers to the high-temperature value; in others, it is lower. The v_{max} values labeling the various curves in Fig. 2A are calculated at the low-temperature limit. This minimum in amplitude is a signature of dissipation and is reminiscent of that found in two-dimensional, thin, superfluid liquid ^{4}He films adsorbed on a planar surface (*17*–*19*). In addition to the minimum, the amplitude also shows a smooth decrease with increasing temperature above 0.3 K. This feature is not related to the dissipation of superflow seen when the torsional cell is filled with solid ^{3}He.

If the resonant period drop is due to solid helium in the annulus entering the supersolid phase, then in the reference frame of the torsional cell the supersolid fraction would be executing oscillatory superflow around the annulus. If a barrier is present in the annulus, superflow around the annulus cannot be established and the decrease in the resonant period should be vastly reduced. The result of this control experiment on a solid sample of 36 bars measured with a cell with a barrier in the annulus is shown in Fig. 2B. Because the physical dimensions of this torsion cell—including the diameter and the width of the (blocked) annulus—are larger than those of the barrier-free or unblocked cell, the expected period shift in the absence of the barrier is also larger. The expected total period shift in the absence of the barrier is 95 ± 15 ns. Instead, a period shift of 1.4 ± 0.2 ns, or 1.5 ± 0.5% of the expected value, is seen. A superfluid sample confined in a finite cavity, due to irrotational flow, will exhibit decoupling even if the cavity does not make a complete path around the axis of rotation (*20*). A calculation of this irrotational flow effect, mimicking the geometry and dimensions of the blocked channel, found a decoupling of 0.8% (*21*), on the order of the measured value. Another possible source of this decoupling is the small gap of several μm that was left unfilled by epoxy resin when the torsion rod was attached to the torsion cell. The reason for this gap is that we wanted to make sure the hole from the torsion rod to the annulus remained open for the introduction of ^{4}He. We estimate that this gap may contribute up to 0.5 ns of the observed decoupling. We repeated the measurement with liquid helium with this blocked cell. The period of oscillation increased by 5270 ns when the annulus was filled with normal liquid. In the low-temperature limit, all the liquid should be superfluid; however, the total decoupling

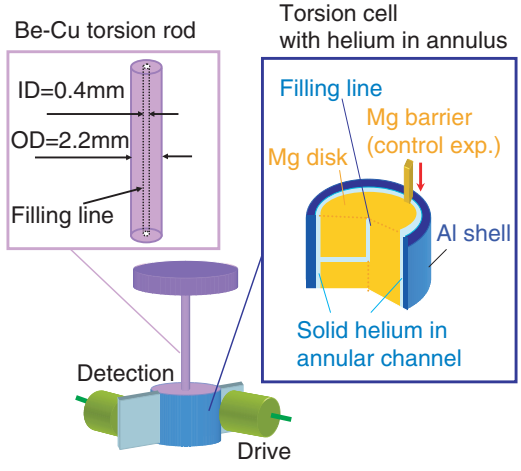

Fig. 1. Torsional oscillators: The cylindrical drive and detection electrodes are coupled capacitively to the two planar electrodes attached as fins on the two sides of the cylindrical torsion cell. Oscillation of the torsion cell induces an ac voltage on the detection electrode. This voltage enables a lock-in amplifier to keep the oscillation in resonance. The outside diameter, width, and height of the channel in the barrier-free torsion cell are 10 mm, 0.63 mm, and 5 mm, respectively. The mechanical quality factor of the oscillator is 2×10^6, allowing the determination of the resonant period to 0.2 ns out of a resonant period of 1 ms. The outside diameter, width, and height of the (blocked) channel of a second torsion cell with the barrier are 15 mm, 1.1 mm, and 5 mm, respectively. The mechanical quality factor and period precision values are similar to those of the barrier-free torsion cell.

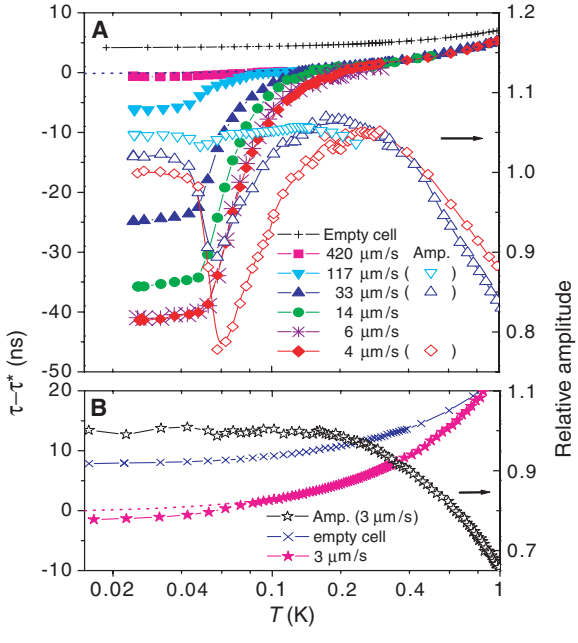

Fig. 2. Resonant period and amplitude of oscillation as a function of temperature for the unblocked (**A**) and blocked (**B**) cell. The period readings are shifted relative to τ^*, the resonant period at 300 mK. The values of τ^* for the open cell with helium are 1,099,477 ns, 1,099,480 ns, 1,099,482 ns, 1,099,483 ns, 1,099,488 ns, and 1,099,485 ns when the maximum oscillation speed are, respectively, 4, 6, 14, 33, 117, and 420 μm/s. The empty-cell period at 300 mK is 1,096,465 ns, 3012 ns less than that when the cell is full. The value of τ^* for the blocked cell with solid helium at 36 bars at 300 mK is 2,242,940 ns. The resonant period when it is empty at 300 mK is 2,235,890 ns.

we observed is only 90 ns. In other words, the observed fractional decoupling in the blocked cell filled with superfluid is comparable to that found for solid helium. This similarity suggests that superflow in solid ^{4}He, as in superfluid, is also irrotational. In contrast to the data obtained with the barrier-free or unblocked cell, there is no observable minimum in the amplitude. We have also made measurements with high-purity (99.999%) solid ^{3}He in the barrier-free torsion cell and found no drop in the resonant period and no amplitude minimum.

In Fig. 3 we plot the nonclassical rotational inertia fraction (*11*) (*NCRIF*) as a function of temperature for 3 of the 17 samples we studied. *NCRIF* is defined as the period shift $\tau - \tau^*$ (Fig. 2A) divided by the increase in period due to the filling of the annulus with the specific ^{4}He sample. The family of curves in Fig. 3, A to C, show *NCRIF* determined with different values of v_{max}. *NCRIF* obtained with v_{max} smaller than a certain critical value, v_c, collapses into a single curve. Exceeding v_c, *NCRIF* is found to decrease with v_{max}. The value of v_c of the samples at 41 and 65 bars (Fig. 3, B and C) and 51 bars (Fig. 2A) is close to 5 μm/s. A much higher v_c, close to 38 μm/s, is found for the 26-bars sample. The value of *NCRIF* in the low-temperature limit (at 20 mK) as a function of v_{max} for five different solid samples is also shown (Fig. 3D). The results shown in Figs. 3 and 2A can be understood by thinking of v_c as the critical velocity of superflow. When the torsional cell is oscillating with v_{max} below v_c, a fraction of the helium (i.e., the supersolid fraction) is stationary and does not contribute to rotational inertia. The collapsed *NCRIF* curves at these low speeds are therefore plots of the supersolid fraction, ρ_s/ρ, as a function of temperature. When the cell is oscillating with v_{max} exceeding v_c, supersolid decoupling occurs only during the portion of the oscillation cycle when the instantaneous speed is less than v_c, and thus gives rise to a smaller *NCRIF* and smaller period shift.

Liquid helium undergoing superflow around an annulus of radius R satisfies the Onsager-Feynman quantized circulation relation (*22*), $2\pi R \cdot v_s = (h/m) \cdot n$, where v_s is the superflow velocity, h is Planck's constant, m is the mass of helium atom, and the integer n is the circulation quantum number. For R = 5 mm, as in our annulus, v_s = 3.6 μm/s for n = 1. The fact that this velocity is on the same order of magnitude as the critical velocity v_c defined above indicates that the decrease in *NCRIF* with increasing v_{max} is associated with the appearance of vortices of a single or few unit(s) of quantum circulation in the superflow.

The temperature dependence of ρ_s/ρ at different pressures—that is, the (collapsed) *NCRIF* curves measured with the lowest speeds (Fig. 3, A to C)—shows a "universal" behavior of a smooth but increasingly rapid rise with decreasing temperature and then a saturation in the low-temperature limit. Thirteen other samples (in addition to the samples featured in Figs. 2 and 3) with pressure falling between 26 and 66 bars, all showing the same "universal" supersolid behavior, were studied with either one or two low oscillation speeds, typically with v_{max} close to or smaller than 5 μm/s. The low-temperature supersolid fraction, ρ_{so}/ρ, for all 17 solid samples (fig. S1) ranges from 0.0075 to 0.0175 and clusters between 0.01 and 0.015. The scatter in the result makes it difficult to conclude whether there is a real trend of increasing ρ_{so}/ρ with pressure. We speculate that the variation in ρ_{so}/ρ is related to the less than ideal crystallinity of the solid helium samples. Given the temperature gradient and different wall materials that exist in the torsional cell and the capillary leading to the cell, solid helium grown by the blocked capillary method is likely to be polycrystalline with grain boundaries that may affect the coherence of the superflow and possibly the magnitude of the supersolid fraction. The largest ρ_{so}/ρ value, 0.017, is comparable to that found for the experiment with helium confined in Vycor (0.025) (*15*). The Vycor value includes a multiplicative factor of 5 to correct for the tortuous pore structure of the Vycor glass. The theoretical estimate of the zero-temperature supersolid fraction varies from 1 part per million to 40% (*11*, *23*–*26*).

In addition to the comparable amplitude, the temperature dependence of the ρ_s/ρ of ^{4}He in Vycor resembles that found in bulk solid samples (*15*). These similarities suggest that the observed superflow in these two systems is an intrinsic low-temperature property of solid helium. One may argue that the decrease in the resonant period is not due to superflow but due to solid helium (with a soft shear mode) not following the acceleration of the torsional cell. This means the viscous penetration depth (δ) of solid helium must be less than 3.5 nm, the typical radius of the pores in Vycor glass. Its viscosity, $\eta = \delta^2\rho\omega$ (where ρ = 0.2 g/cc and $\omega = 2\pi \cdot 1024$ Hz are the density of solid helium and the angular frequency of the torsional motion, respectively), must be less than 1.5×10^{-11} Pa·s.

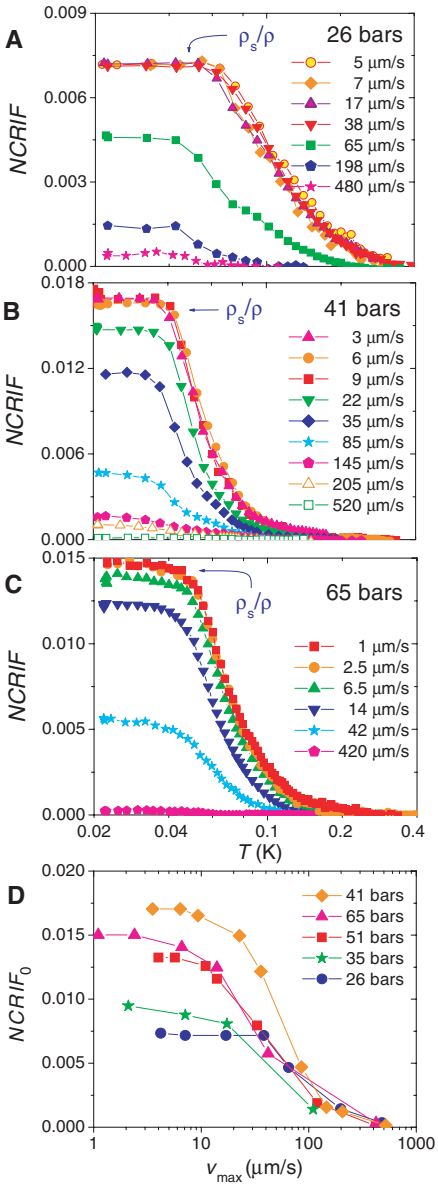

Fig. 3. (A to C) *NCRIF* as a function of temperature for three solid samples at different maximum oscillation speeds v_{max}. The observed period increases due to filling of the cell with ^{4}He at 300 mK are, respectively, 2785 ns, 2886 ns, and 3143 ns for solid samples at 26, 41, and 65 bars. *NCRIF* curves measured with oscillation speed less than the critical velocity of superflow collapse into a single curve. These curves represent the supersolid fraction, ρ_s/ρ, as a function of temperature. (**D**) *NCRIF* in the low-temperature limit as a function of v_{max}.

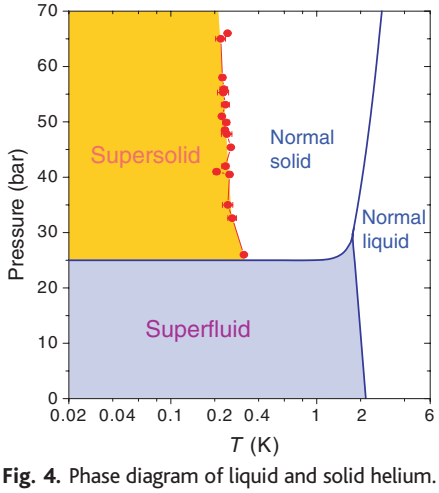

Fig. 4. Phase diagram of liquid and solid helium.

This number is one-seventh of the value reported in (*1*) as the upper limit of viscosity of superfluid helium. For comparison, the viscosity of normal fluid ^{4}He is 2×10^{-6} Pa·s. This calculation invalidates this soft shear mode interpretation and supports the superflow interpretation.

The smooth decay in ρ_s/ρ with increasing temperature near 250 mK makes it difficult to determine with precision the supersolid transition temperature T_c. We estimate the value of T_c by assuming a linear dependence of ρ_s/ρ on temperature near T_c and then use the data with ρ_s/ρ between 0.01 and 0.1 to fit for T_c. The resultant transition temperatures, with uncertainty of 20 mK, are likely to be lower than the "true" values. The transition temperatures we have found show a weak pressure dependence decreasing from 315 mK at 26 bars down to 230 mK at pressures exceeding 40 bars. The phase diagram of ^{4}He, including both the superfluid and supersolid phases, is shown in Fig. 4.

A number of experiments have searched for the supersolid phase in bulk solid helium without success (*27*). A recent experiment found an unexpected interaction between acoustic and heat pulses in solid ^{4}He with several tens of parts per million of ^{3}He (*28*). The result led to the interpretation of a Bose condensate of thermally activated vacancies at temperatures above 200 mK and therefore is not related to the findings reported here. A prior torsional oscillator experiment (*29*) reported the absence of any supersolid decoupling in a solid ^{4}He sample that contains 411 parts per million of ^{3}He—a concentration, as we found in the Vycor experiment (*15*), sufficient to quench the supersolid phase. The authors of this prior experiment also reported that they failed to find evidence of the supersolid phase in samples of high-purity ^{4}He (*29*). Our results disagree with this conclusion. Other experiments involve the search of motion of a falling dense object in solid helium or flow of solid helium from one chamber of higher pressure to one of lower pressure (*30–34*). A likely explanation of why these experiments found null results is that such pressure-driven mass flow requires a difference in the supersolid fraction between regions or chambers of different pressures. Our measurements showed that the supersolid fraction is insensitive to the pressure of the solid ^{4}He samples.

We noted above that Bose-Einstein condensation is found together with superfluidity in bulk liquid helium and in alkali gases. In contrast, superfluidity at $T > 0$ is found in two-dimensional liquid helium films without Bose-Einstein condensation (*18*). An intriguing question is whether the supersolid phase is associated with Bose-Einstein condensation.

References and Notes

1. P. Kapitza, *Nature* **141**, 74 (1938).
2. J. F. Allen, A. D. Misener, *Nature* **141**, 75 (1938).
3. P. Nozières, D. Pines, *Theory of Quantum Liquids* (Addison-Wesley Reading, MA, 1989), vol. 2, chap. 6.
4. P. E. Sokol, in *Bose-Einstein Condensation*, A. Griffin, D. W. Snoke, S. Stringari, Eds. (Cambridge Univ. Press, Cambridge, 1995).
5. M. Anderson, J. R. Ensher, M. R. Matthews, C. E. Wieman, E. A. Cornell, *Science* **269**, 198 (1995).
6. M. R. Matthews *et al.*, *Phys. Rev. Lett.* **83**, 2498 (1999).
7. A. P. Chikkatur *et al.*, *Phys. Rev. Lett.* **85**, 483 (2000).
8. F. Chevy, K. W. Madison, J. Dalibard, *Phys. Rev. Lett.* **85**, 2223 (2000).
9. A. F. Andreev, I. M. Lifshitz, *Sov. Phys. JETP* **29**, 1107 (1969).
10. G. V. Chester, *Phys. Rev. A.* **2**, 256 (1970).
11. A. J. Leggett, *Phys. Rev. Lett.* **25**, 1543 (1970).
12. K. S. Liu, M. E. Fisher, *J. Low Temp. Phys.* **10**, 655 (1973).
13. M. Liu, *Phys. Rev. B* **18**, 1165 (1978).
14. D. E. Galli, L. Reatto, *J. Low Temp. Phys.* **124**, 197 (2001).
15. E. Kim, M. H. W. Chan, *Nature* **427**, 225 (2004).
16. J. R. Beamish, *Nature* **427**, 204 (2004).
17. D. J. Bishop, J. D. Reppy, *Phys. Rev. Lett.* **40**, 1727 (1978).
18. J. M. Kosterlitz, D. J. Thouless, *J. Phys. C* **6**, 1181 (1973).
19. V. Ambegaokar, B. I. Halperin, D. R. Nelson, E. D. Siggia, *Phys. Rev. Lett.* **40**, 783 (1978).
20. A. L. Fetter, *J. Low Temp. Phys.* **16**, 533 (1974).
21. E. J. Mueller, personal communication.
22. R. P. Feynman, in *Progress in Low Temperature Physics I* (North-Holland, Amsterdam, 1955), chap. 2.
23. J. F. Fernandez, M. Puma, *J. Low Temp. Phys.* **17**, 131 (1974).
24. R. A. Guyer, *Phys. Rev. Lett.* **26**, 174 (1970).
25. W. M. Saslow, *Phys. Rev. Lett.* **36**, 1151 (1976).
26. D. Ceperley, G. V. Chester, M. H. Kalos, *Phys. Rev. B* **17**, 1070 (1978).
27. M. W. Meisel, *Physica B* **178**, 121 (1992).
28. J. M. Goodkind, *Phys. Rev. Lett.* **89**, 095301 (2002).
29. D. J. Bishop, M. A. Paalanen, J. D. Reppy, *Phys. Rev. B* **24**, 2844 (1981).
30. A. Andreev, K. Keshishev, L. Mezhov-Deglin, A. Shal'nikov, *Pis'ma Zh. Eksp. Teor. Fiz.* **9**, 507 (1969) [*Sov. Phys. JETP Lett.* **9**, 306 (1969)].
31. V. L. Tsymbalenko, *Pis'ma Zh. Eksp. Teor. Fiz* **23**, 709, (1976) [*Sov. Phys. JETP Lett.* **23**, 653 (1976)].
32. D. S. Greywall, *Phys. Rev. B* **16**, 1291 (1977).
33. G. Bonfait, H. Godfrin, B. Castaing, *J. Phys. (Paris)* **50**, 1997 (1989).
34. N. E. Dyumin, S. V. Svatko, V. N. Grigor'ev, *Fiz. Nizk. Temp.* **15**, 524 (1989).

35. We thank J. R. Banavar, J. R. Beamish, D. J. Bishop, M. E. Fisher, J. M. Goodkind, J. K. Jain, A. J. Leggett, E. Mueller, M. A. Paalanen, J. D. Reppy, W. M. Saslow, K. Shirahama, and D. S. Weiss for informative discussions. Supported by the NSF Condensed Matter Physics Program.

Supporting Online Material

www.sciencemag.org/cgi/content/full/1101501/DC1
Fig. S1

15 June 2004; accepted 12 August 2004
Published online 2 September 2004;
10.1126/science.1101501
Include this information when citing this paper.

Visualization of Dislocation Dynamics in Colloidal Crystals

Peter Schall,[1]* Itai Cohen,[1,2] David A. Weitz,[1,2] Frans Spaepen[1]

The dominant mechanism for creating large irreversible strain in atomic crystals is the motion of dislocations, a class of line defects in the crystalline lattice. Here we show that the motion of dislocations can also be observed in strained colloidal crystals, allowing detailed investigation of their topology and propagation. We describe a laser diffraction microscopy setup used to study the growth and structure of misfit dislocations in colloidal crystalline films. Complementary microscopic information at the single-particle level is obtained with a laser scanning confocal microscope. The combination of these two techniques enables us to study dislocations over a range of length scales, allowing us to determine important parameters of misfit dislocations such as critical film thickness, dislocation density, Burgers vector, and lattice resistance to dislocation motion. We identify the observed dislocations as Shockley partials that bound stacking faults of vanishing energy. Remarkably, we find that even on the scale of a few lattice vectors, the dislocation behavior is well described by the continuum approach commonly used to describe dislocations in atomic crystals.

Dislocations in a crystalline lattice are central to our understanding of yield, work hardening, fracture, fatigue, and time-dependent elasticity in atomic crystals (*1*). Such dislocations are line defects that mark the boundary of a surface at which one part of the crystal has been uniformly translated with respect to the other (*2–4*). A complete understanding of dislocations and their dynamics requires an analysis that bridges a range of length scales (*5*). On the atomic scale, the interatomic potential determines the structure of the dislocation core. On the medium-range scale, the strain field of the dislocations determines their interactions. On the macroscopic scale, the behavior of the dislocations determines the deformation of the crystal. It is difficult to observe dis-

[1]Division of Engineering and Applied Sciences, [2]Department of Physics, Harvard University, 9 Oxford Street, Cambridge, MA 02138, USA.

*To whom correspondence should be addressed. E-mail: pschall@deas.harvard.edu